JOURNAL OF AIRCRAFT
Vol. 31, No. 1, Jan.–Feb. 1994

Characteristics of the Surface Pressures on a F/A-18 Vertical Fin Due to Buffet

B. H. K. Lee* and F. C. Tang†
Institute for Aerospace Research, Ottawa, Ontario, K1A 0R6 Canada

A wind-tunnel investigation of the characteristics of the surface pressures on the vertical fin of a rigid 6% scale model of the F/A-18 due to buffet has been conducted in the Institute for Aerospace Research (IAR) 1.5-m trisonic blowdown wind tunnel. The measurements were carried out by means of 48 fast response pressure transducers installed directly opposite to each other on the fin surfaces. Time-averaged and rms pressure distributions at various angles of attack were determined to investigate the behavior of the pressures on the fin surfaces. Space-time correlations of the transducer signals were performed to obtain the broadband eddy scale and convection pattern of the pressure field. The buffet loads were calculated from summation of the pressure signals on the vertical fin surfaces. Spectral analyses and probability densities were evaluated to provide statistical information on the characteristics of the buffet loads.

Nomenclature

A_j = area of jth panel on vertical fin
A_T = total surface area of fin
C_N = vertical fin normal force coefficient, positive outboard
C_p = time-averaged pressure coefficient
C'_p = rms value of pressure coefficient, p_{rms}/q
$\bar{c}$ = wing mean aerodynamic chord, 210.56 mm
$\bar{c}_f$ = vertical fin mean aerodynamic chord, 127.7 mm
f = frequency
k = nondimensional frequency, $f\bar{c}/U_\infty$
M = freestream Mach number
p_I = pressure on vertical fin inboard surface
p_O = pressure on vertical fin outboard surface
p_{rms} = rms value of pressure
q = freestream dynamic pressure
$R(a, b, \tau)$ = correlation of functions a and b
$R_{e\bar{c}}$ = Reynolds number based on $\bar{c}$
s = distance measured along a constant chord line on vertical fin
U_∞ = freestream velocity
x_f = distance measured along a constant span line on vertical fin
α = angle of attack
τ = time delay

I. Introduction

THE F/A-18, through the use of advanced digital flight control systems, the optimized positioning of the horizontal and vertical fins, and its multiple high-lift aerodynamic devices can sustain controlled flight up to 50-deg angle of attack. Its enhanced agility has resulted in the development of air combat maneuver tactics focused on high-angle-of-attack regimes.

The leading-edge extension (LEX) is prominent among high-lift devices and has been credited with a large increase in maximum lift over that which would be obtained without the LEX. An increase of 22% in maximum lift and a delay of 10 deg in the angle of attack for maximum lift can be achieved. Maneuverability in this flow regime is also enhanced by the interaction of the vortical flow with the tail control surfaces.

The major drawback of the LEX is the large buffet loads that the vertical fins of the aircraft are being subjected to. Structural integrity of the vertical fins is currently a major concern for high-performance fighter aircraft, especially those with twin tails configuration. The rolled-up vortices that originate from the sharp edge of the F/A-18 LEX ultimately burst. The resulting highly turbulent flow upon impact on the tail causes severe structural damage. Peak accelerations up to 450g measured at a position close to the tip of the vertical fin have been reported from flight tests at the Aerospace Engineering Test Establishment at Cold Lake.[1] Some alleviation of buffet loads has been achieved through a modification of the LEX by the addition of a streamwise fence. Reference 1 also reports the efficacy of the LEX fences in reducing the peak accelerations to 200 g.

Some results of an investigation of tail buffet on a rigid 6% scale model of the F/A-18 carried out in the transonic test section of the Institute for Aerospace Research 1.5-m trisonic blowdown wind tunnel have been reported in Refs. 1 and 2. The flowfield behind the vertical fin was investigated using a vortex rake with 49 pitot-pressure tubes to measure the steady and unsteady pressures.[3] Spectral analysis and cross-correlation studies were also performed. Analysis of peak buffet loads on the vertical fin was carried out using extreme value statistics.[4] These investigations are useful to understand the flow phenomena near the vertical fin and the correlation between pressure fluctuations in the flowfield with those on the fin.

In this article, results on the measurements of vertical fin surface pressures are presented. Time-averaged and rms pressure distributions were determined in order to obtain a better understanding of the behavior in the flow characteristics on both sides of the fin. The pressure difference across the fin was computed in order to calculate the normal force. Tests were carried out at different Mach numbers and angles of attack, but only results at $M = 0.6$ are presented. Mach number effects will be addressed in a later article. The Reynolds number and dynamic pressure are 3.38×10^6 and 3.95 psi, respectively. Results for three angles of attack at 25, 30, and 35 deg are presented. These values of α are of particular

Received Dec. 18, 1991; presented as Paper 92-2127 at the AIAA Dynamic Specialist Conference, Dallas, TX, April 16–17, 1992; revision received Aug. 28, 1992; accepted for publication Sept. 15, 1992.

*Senior Research Officer, National Research Council, High Speed Aerodynamics Laboratory. Associate Fellow AIAA.
†Associate Research Officer, High Speed Aerodynamics Laboratory.

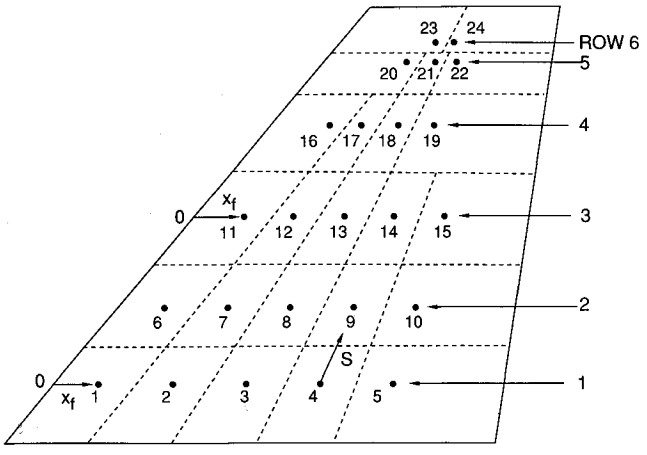

Fig. 1 Fin pressure transducer locations.

interest in high-angle-of-attack tail buffeting studies. Reference 3 shows that the position of the time-averaged center of the vortical flow is near the outboard surface of the vertical fin at $\alpha = 25$ deg and in its vicinity at $\alpha = 30$ and 35 deg.

II. Model and Instrumentation

The model used was a sting-mounted 6% scale of the F/A-18 with streamwise fences installed. It consists of three major pieces,[1] namely an aluminum alloy nose section, with integral LEX equipped with removable fences and a single place canopy, a stainless-steel center fuselage with integral wings, and a stainless-steel rear fuselage. The center fuselage is bored to accept a 38.1-mm-diam Able Corp. sting balance.

Leading- and trailing-edge flaps are fastened to the wings by simple bolted lap joints with dowel pins for accurate assembly. In the model tested, the leading- and trailing-edge flaps were deflected at 35 and 0 deg, respectively, and the horizontal stabilator angle was set at -9 deg. These settings correspond closely to those obtained from flight tests at the angles of attack investigated in the wind-tunnel tests.

Through-flow air intakes and flow passages are provided with removable internal chokes. The flow passages terminate in D-shaped exits on each side of the support sting. Models of the AIM 9 missiles were fixed to the wing tips for the measurements.

The starboard fin was instrumented to measure unsteady pressures at 24 positions directly opposite to each other on each surface. Figure 1 shows the locations of the pressure transducers on the fin surface and their coordinates are given in Ref. 1.

Boundary-layer transition trips were installed in the manner as described in Ref. 5. Rows of epoxy cylinders (1.143-mm diam on 2.54-mm centers, 0.0508 mm high) were applied 10.16 mm behind the leading edges of the LEX, wings, intakes, vertical fins, and horizontal stabilators, on both surfaces. In addition, a ring was applied around the nose, 10.16 mm behind the tip, and a longitudinal row was fixed on the underfuselage centerline from nose to the intakes' station.

III. Results and Discussion

A. Vertical Fin Time-Averaged Pressure Distribution

The advantage of using rigid model pressure measurements to predict buffet response of a flexible aircraft is that structural modifications can be incorporated in the early design stages so that severe buffeting can be avoided. The methods described in Refs. 6 and 7 require a large number of pressure measurements to be made on the inboard and outboard surfaces of the vertical fin. The optimum locations and spacings of the pressure transducers require a good understanding of the characteristics of the pressure field on the fin surfaces. Proper choice of these two parameters will reduce the number of pressure transducers required at a saving in cost and the time required to reduce the large amount of data acquired during a wind-tunnel test.

Results of the vortical flow time-averaged total pressure contours were reported in Ref. 3. At $M = 0.6$ and $\alpha = 25$ deg, the center of the low-pressure region is located outboard of the vertical fin. Increasing α to 30 deg, the measurements show that the vortex core moves closer to the fin and a small low-pressure region is present on the inboard side of the fin. At $\alpha = 35$ deg the low-pressure region increases in size and the vortex structure shifts upwards. In this article results for these three values of α are given since they represent the flow phenomena that are of interest in high α tail buffet studies.

The pressure distributions on the inboard and outboard surfaces of the vertical fin were shown in Ref. 8 in graphical form. Time-averaged and rms pressure coefficients were plotted along the chordwise- and spanwise-directions for three values of the angle of attack to show the effect of the location of the vortex burst position on pressure distributions. The graphs contain a great deal of information on the pressure variations with angle of attack, but are too detailed for presentation in a journal publication. The results in Ref. 8 are reproduced in this article in the form of color contour plots in order to give an overview of the behavior of the pressure field.

Figure 2 shows the time-averaged C_p contours on the inboard surface at $M = 0.6$ and $\alpha = 25$, 30, and 35 deg. The two lower corner points in each of the figures correspond to transducers 1 and 5, respectively (Fig. 1). The sixth row of transducers was not used to construct the contour plots, since only two transducers were available and they are quite close to the fifth row of transducers. On the fifth row, there are only three transducers, and the data at the two upper corner points in the figures are obtained from extrapolation using the rows of transducers in the chordwise- and spanwise-directions, respectively. There is also one point along the fourth row of transducers on the trailing-edge side that is obtained in the same manner.

When the vortex burst position is far upstream of the vertical fin, e.g., at $\alpha = 30$ and 35 deg, the time-averaged C_p values on the fin surfaces are quite close to each other. As α decreases, the burst position moves closer to the vertical fin and the differences in C_p increase and become more noticeable in the figures.

Near the fin root, the pressure is higher than that on the rest of the fin with the largest values being detected near the leading edge. The pressure decreases towards the trailing edge in the chordwise-direction. From approximately midspan to

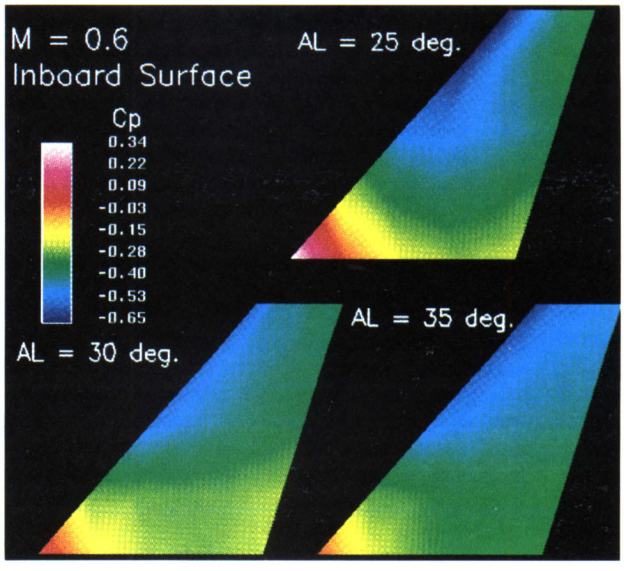

Fig. 2 C_p contours on vertical fin inboard surface.

the fin tip, the lowest pressure is found near the leading edge and it increases gradually towards the trailing edge.

The changes in C_p in the spanwise direction are quite similar at $\alpha = 30$ and 35 deg in a region covering an area from the leading edge to nearly 50% chord. Between 50% chord and the trailing edge, the time-averaged pressure is found to be slightly higher at $\alpha = 30$ deg.

The largest difference in the measurements between $\alpha = 25$ deg and those at $\alpha = 30$ and 35 deg is detected near the fin root close to the leading edge. For the greater part of the fin, some small differences in pressure distributions can be found among the three values of α, and they are more easily detected when plotted in graphical form as shown in Ref. 8.

In Fig. 3, the time-averaged pressure contours are shown for the outboard surface. The C_p scale is different from that in Fig. 2. The pressures are, in general, lower than those on the inboard surface. At $\alpha = 25$ deg, the values of C_p are higher than those obtained at $\alpha = 30$ and 35 deg. At this value of α, the center of the vortex measured from the time-averaged total pressure contours is located on the outboard side of the fin.[3] The locations of the regions of maximum and minimum pressure at these three values of incidence are quite different from those found on the inboard surface. The lowest pressure is measured near the leading edge close to the fin root, and the highest pressure is found close to the trailing edge at the fin tip. Unlike the inboard surface, the pressure near the fin root is lower than that on the rest of the fin. C_p increases both in the chordwise- and spanwise-directions. The difference in the pressure distribution shown in Figs. 2 and 3 is due primarily to the very different flow pattern on the two surfaces. This has been shown from tuft photographs and videotapes of the flowfields on the inboard and outboard surfaces of the NASA high-alpha research vehicle[9] and surface streamlines from oil dots experiments.[1] Further discussion on the flow behavior is given in Sec. III.C.

B. Vertical Fin rms Pressure Distribution

The rms values of the pressure fluctuations C_p' on the vertical fin inboard surface are shown in Fig. 4 for the same test conditions as Figs. 2 and 3. The magnitude of the pressure fluctuations increases with angle of attack. Close to the leading edge of the fin, the fluctuations are higher and they decrease towards the trailing edge. At $\alpha = 30$ and 35 deg there is a region in the vicinity of the midspan of the fin where the values of C_p' are the largest. This type of behavior in C_p' is not detected at $\alpha = 25$ deg where most of the pressure fluctuations are very low, except near the fin tip. Here, C_p' approaches values close to those obtained for the higher α cases.

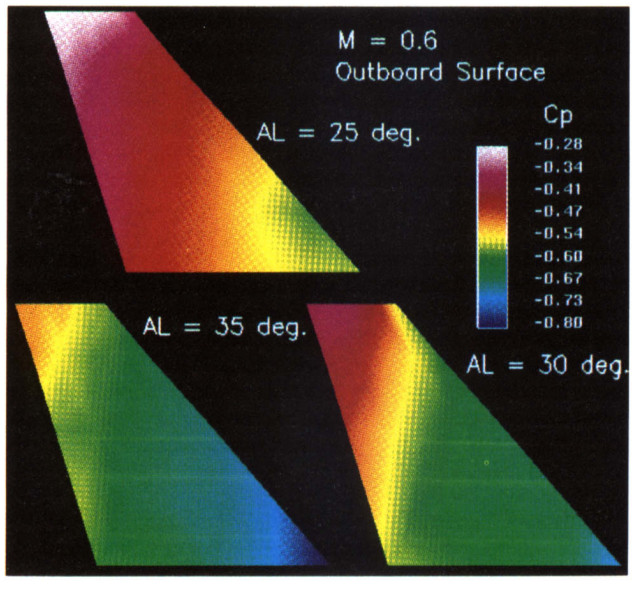

Fig. 3 C_p contours on vertical fin outboard surface.

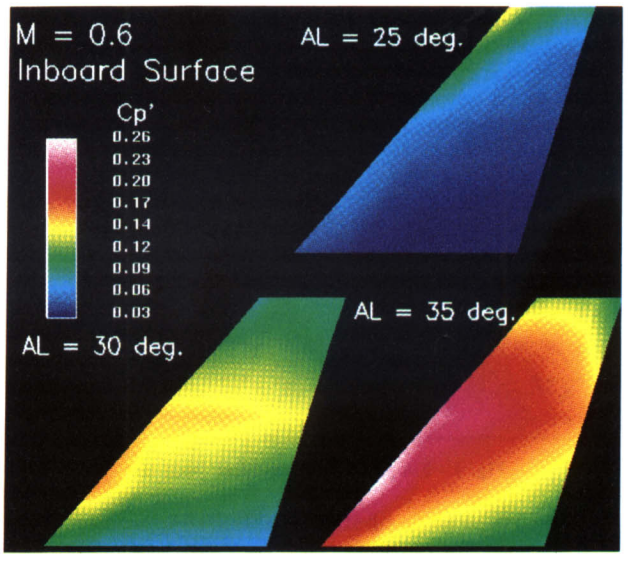

Fig. 4 C_p' contours on vertical fin inboard surface.

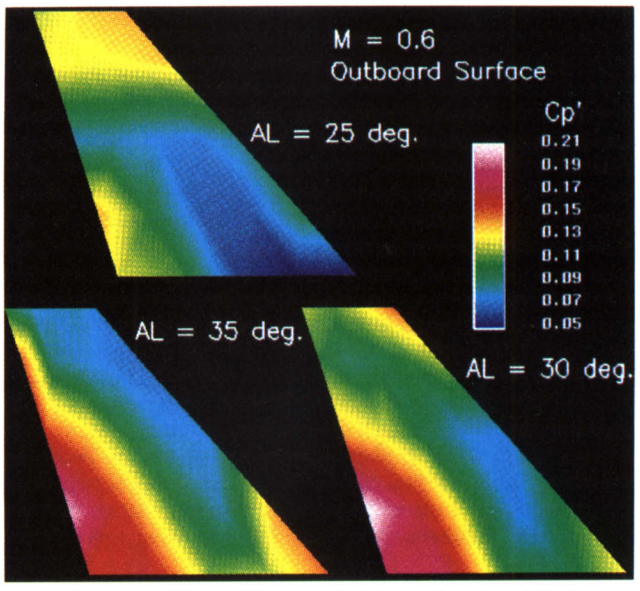

Fig. 5 C_p' contours on vertical fin outboard surface.

On the outboard surface, Fig. 5 shows that the difference in pressure fluctuation intensity between $\alpha = 30$ and 35 deg is small up to the third row of pressure transducers. An increase in C_p' from the leading edge towards the trailing edge is observed, and a maximum is found in a region covering an area from approximately 50% chord to the trailing edge and from the fin root to 50% span. The figure shows the differences in C_p' between $\alpha = 30$ and 35 deg are larger close to the fin tip.

Up to the third row of transducers the values of C_p' at $\alpha = 25$ deg are below those for the two higher angles of attack considered. From the third to the fifth row of transducers, larger values of the pressure fluctuations are observed. Comparison with results obtained at $\alpha = 30$ and 35 deg shows that the pattern of the intensity of the unsteady pressure fluctuations to be very different. The position of the vortex center accounts for the behavior in the pressure fluctuations observed in the figures.

C. Space-Time Pressure Correlation

Broadband space-time correlation of the pressures on both surfaces of the fin was carried out using the IEEE CCSE cross-correlation algorithm.[10] An example of the space-time

cross-correlation using the transducer 6 (Fig. 1) as the reference and forming pairs such as transducers 6 and 7, 6 and 9, etc., is shown in Fig. 6 for the inboard surface at $M = 0.6$ and $\alpha = 30$ deg. The horizontal scale is τ (in ms) relative to the reference transducer when the peak correlation function is detected at the transducer position where correlation is computed. The correlation function is normalized with respect to the peak autocorrelation function of transducer 6. Broadband convection velocities of the eddies in the pressure field along the x_f direction can be determined knowing the spatial separation between transducers and τ. In this particular example, the velocity is approximately 72% of the freestream velocity. For the third row of transducers using transducer 11 as the reference, a different convection velocity of the pressure field was obtained. A distinct pattern of convection along the chord direction was not observed near the fin root and fin tip.

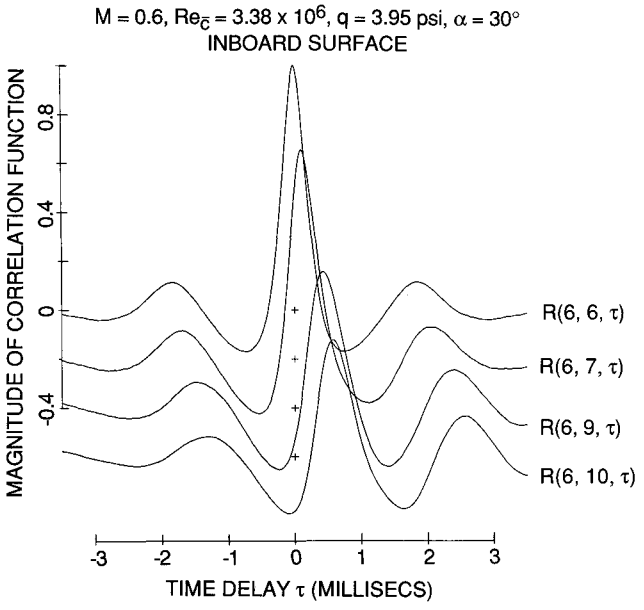

Fig. 6 Cross-correlation functions along second row of transducers on vertical fin inboard surface.

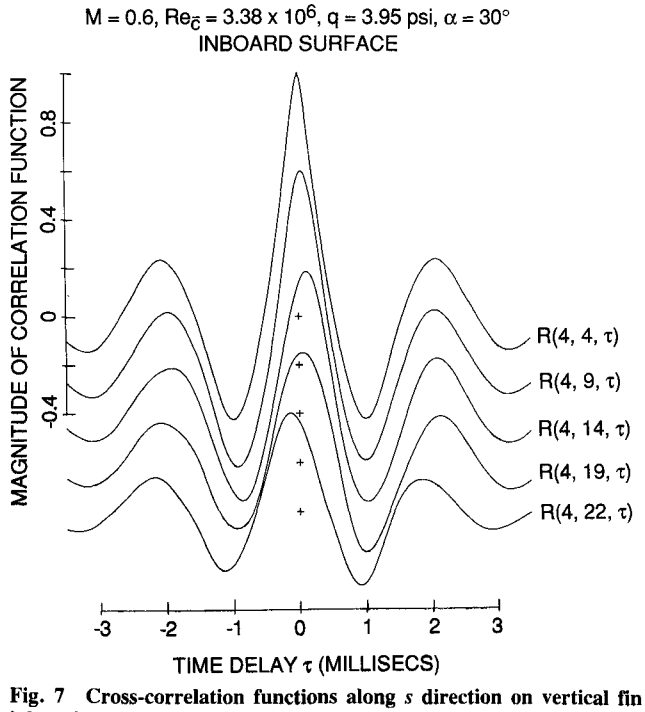

Fig. 7 Cross-correlation functions along s direction on vertical fin inboard surface.

Carrying out correlation analysis along the constant chord lines in the s direction (Fig. 1), e.g., along the line joining the transducers 4, 9, 14, 19, and 22, it was found that the peaks occur at a time delay approximately zero as shown in Fig. 7. This indicates the pressure field to be convected downstream mainly in the x_f direction.

On the outboard surface, the eddies are being convected mainly in the s direction. Along the line joining the transducers, 4, 9, 14, 19, and 22, which is opposite to the line on the inboard surface where cross-correlation was carried out in Fig. 7, the space-time cross-correlation curves look similar to those given in Fig. 6. The convection velocity is found to be approximately $0.44U_\infty$. The convection pattern of the pressure field on the fin surfaces is found to be very different.

Using one of the transducers close to the center of the fin as reference, e.g., number 9 (Fig. 1) on the inboard surface and number 13 on the outboard surface, cross-correlation was performed using all 48 transducers and the time delay was determined. By interpolating between the values of τ obtained from the transducers, the contours of the peak correlation function can be drawn at different time delays. From the contour lines, it is possible to deduce the convection velocities of the broadband eddies and determine the convection pattern of the pressure field on the vertical fin surfaces.

Figure 8 shows the results at $\alpha = 25$ deg for the inboard and outboard surfaces. On the inboard surface, convection was found mainly in a region occupying approximately $\frac{1}{3}$ of the top part of the fin. The pressure field moves in a direction from the trailing to leading edge of the fin. On the outboard surface, correlation of the pressure field was detected also on an area occupying the upper $\frac{1}{3}$ of the fin. The convection in this case is mainly in the downstream direction.

Flow visualization with tufts was carried out by Fisher et al.[9] at Dryden Flight Research Facility on the F-18 high-alpha

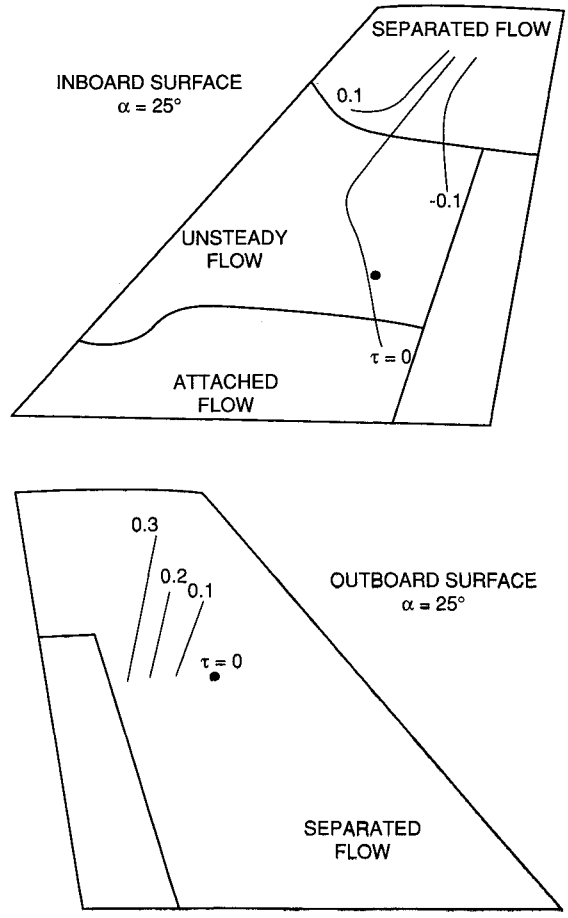

Fig. 8 Peak correlation contours at $M = 0.6$ and $\alpha = 25$ deg.

research vehicle. From the photographs and videotapes of the tufts' motion, they identified three types of flow: 1) attached, 2) unsteady, and 3) separated flows on the vertical fin surfaces. The definition of the three types of flow are as follows: 1) attached flow is observed when the tufts are generally stationary in the direction of flow; 2) unsteady flow occurs when the tufts are fluctuating in the flow direction; and 3) separated flow is identified when the tufts' motion is random. At small angles of attack less than 10 deg, the flow on the fin surfaces is attached. As α increases, areas of unsteady and separated flows begin to appear. At α = 25 deg, the flow on the inboard surface contains regions of attached, unsteady, and separated flows which are marked on Fig. 8. The flow on the outboard surface is completely separated.

Using the results from Ref. 9 at α = 30 deg, Fig. 9 shows that the area of unsteady flow on the inboard surface increases. The area of separated flow on the top part of the fin remains approximately the same as that for α = 25 deg, but now it has increased to include the region near the fin leading edge. A smaller attached flow region near the fin root is observed. There is a much larger area where pressure correlation is observed. The convection in the unsteady region (no convection pattern was detected at α = 25 deg) is mostly in the chordwise-direction. In the separated flow region, there is a strong inflow component of the convection velocity. On the outboard surface of the fin, the flow is fully separated except for a small region near the root where the flow is unsteady. The convection pattern from the cross-correlation of the pressure signals changes slightly compared to that shown in Fig. 8, but the area where correlation is found has increased.

Increasing α to 35 deg, Fig. 10 shows some changes in the convection pattern compared to that at α = 30 deg near the upper part of the inboard surface of the fin. The flow in the midspan of the fin is mainly in the freestream direction. The outboard surface peak correlation lines are similar to those at α = 30 deg, but the region where correlation is observed covered nearly the whole fin surface. The classification of the flow regions shown in the figure is taken from Fisher et al.[9] report for α = 37 deg, but no data was available on the inboard surface. At α = 35 deg, the flow is probably fully separated.

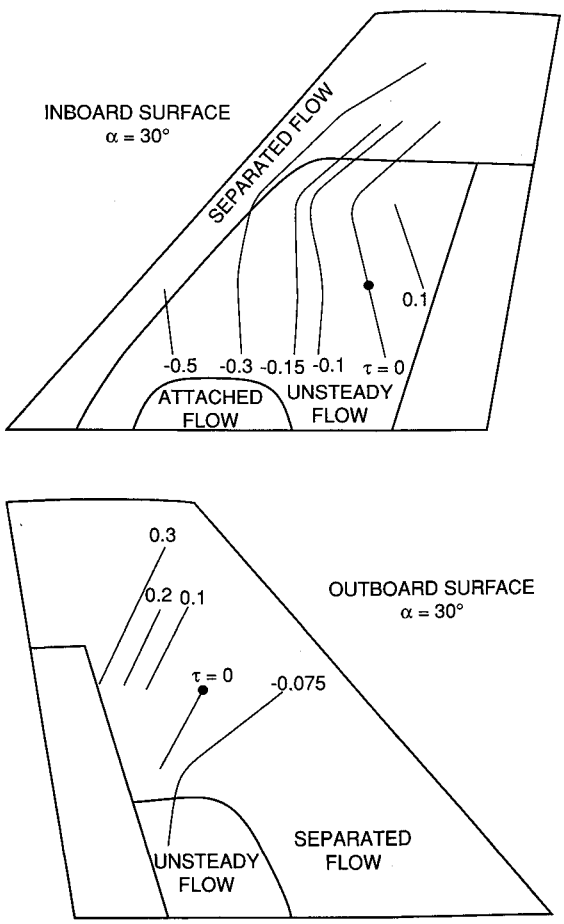

Fig. 9 Peak correlation contours at M = 0.6 and α = 30 deg.

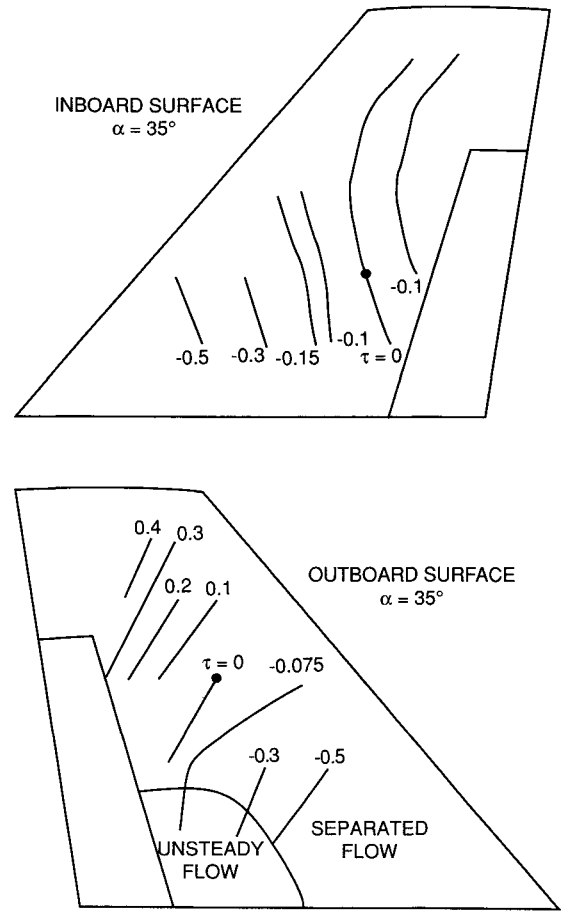

Fig. 10 Peak correlation contours at M = 0.6 and α = 35 deg.

It is not possible to deduce from the present results whether there is a relation between the time-averaged and convected pressure fields on the fin surfaces. An interesting observation is found on the outboard surface where the propagation of the convective pressure field is in a direction which follows the gradient of the time-averaged C_p contours. From the rms pressure measurements, it is seen that on the inboard surface, the values of C_p' are small at α = 25 deg, but there are areas in the unsteady and separated flow regions at α = 30 and 35 deg where pressure fluctuations are large. The attached flow region has small values of C_p'. On the outboard surface, unsteady flow is observed at α = 30 and 35 deg. Large pressure fluctuations are measured in these regions, but unlike the separated flow region, they are not correlated.

The peak correlation functions normalized with respect to the peak auto-correlation function of the reference pressure transducer along constant chord and constant span directions are shown in Figs. 11 and 12 at α = 30 deg. Similar results are obtained for α = 25 and 35 deg, but they are not included in this article. In turbulent flow studies, the scale of the broadband eddies is usually defined to be equal to the distance from the reference transducer to a point on the peak correlation curve where the correlation function decreases to a value of $1/e$ of the reference transducer. On the inboard surface, Fig. 11 shows the eddy scale to vary between 55.8 mm ($0.43\bar{c}_f$) to 114.3 mm ($0.89\bar{c}_f$) in the s direction, and 55.8 mm ($0.43\bar{c}_f$) to

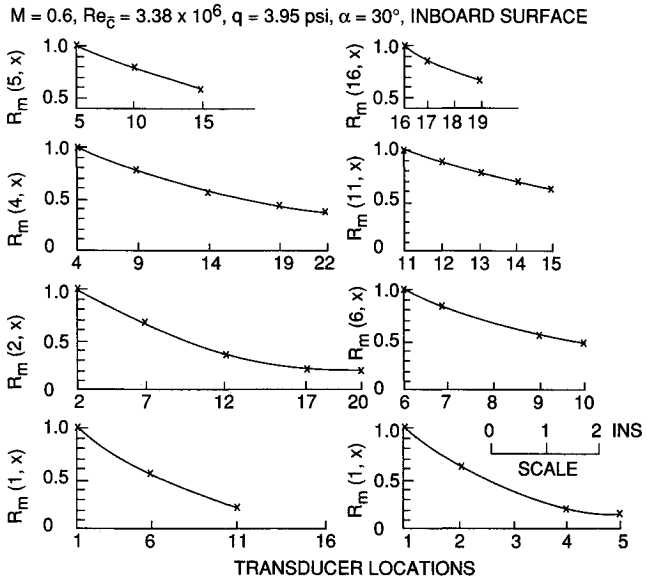

Fig. 11 Normalized peak correlation functions on vertical fin inboard surface.

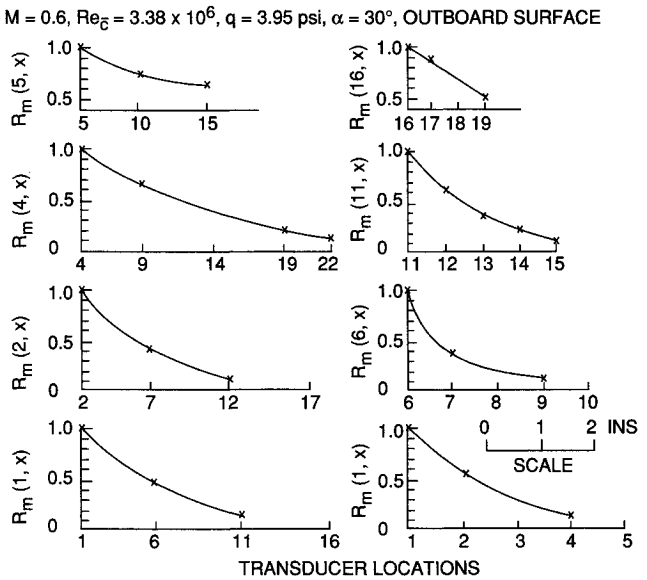

Fig. 12 Normalized peak correlation functions on vertical fin outboard surface.

111.7 mm ($0.87\bar{c}_f$) in the x_f direction. The eddy size is approximately the same in both directions.

On the outboard surface (Fig. 12), the scale varies between 38.1 mm ($0.29\bar{c}_f$) to 63.5 mm ($0.49\bar{c}_f$) in the s direction, and from 20.3 mm ($0.16\bar{c}_f$) to 44.4 mm ($0.34\bar{c}_f$) in the x_f direction. The eddies are slightly larger in the spanwise-direction than in the chordwise-direction. The transducers are not spaced sufficiently close to give very accurate spatial resolution. It is not known at present the reason for the difference in eddy scale on the two surfaces.

Measurements of the pressure field behind the vertical fin[3] show that in the plane approximately normal to the flow, the broadband eddy scale varies between $0.1-0.28\bar{c}_f$. No measurements were made of the scale in the streamwise direction. Correlation between the eddy scale on the fin and that in the flowfield requires more detailed measurements with better spatial resolutions. It is possible to obtain accurate eddy scale on the fin by the installation of additional pressure transducers. However, in the flowfield it is more difficult to do so. The design of the pitot-pressure rake used in Ref. 3 was a compromise between spatial resolution and acceptable blockage effects. The addition of more pitot probes in the rake to give better accuracy of the eddy scale will alter the flowfield significantly and introduce large errors in the measurements.

D. Buffet Loads from Pressure Summation

Discussions on spectral analysis of buffet loads given in Refs. 6 and 7 are based on pressure measurements from transducers installed at one location on the fin. Reference 6 used a pair of transducers on both surfaces at 60% span and 45% chord, while in Ref. 13 only one transducer was placed at 64% chord and 90% span on the outboard surface. From the discussion of the pressure field (Figs. 2–5), it is seen that an analysis based on the pressure transducer output at one location may not be representative of the behavior of the buffet load. Also, the frequency content of the buffet load spectra depends on the transducer position. It was shown in Ref. 11 that there is a variation of the center frequency of the peak in the pressure power spectra from transducers placed on both fin surfaces of a full-scale F/A-18 in the NASA Ames 80- × 120-ft wind tunnel. An accurate description of the load characteristics can only be obtained from analyzing the buffet load calculated from summation of a large number of pressure transducers on the fin surfaces.

Using the fin inboard and outboard surface pressure measurements, the resulting normal force expressed in coefficient form is obtained by the following equation:

$$C_N = \sum_{j=1}^{24} (p_{Ij} - p_{Oj}) A_j / q A_T \qquad (1)$$

The areas A_j of the panels are shown in Fig. 1. It is assumed that the pressure measured by each transducer is constant throughout the panel. The variations of the time-averaged and rms values of the normal force coefficient with α are reported in Ref. 12. In this article, two statistical properties which are useful in structural load analysis are described.

The power spectral density of the normal force is shown in Fig. 13 for the three values of α considered in the previous sections. The IEEE routine PMPSE[10] was used to compute power spectral density. The data were digitized from FM tapes and have an equivalent sampling frequency of 80 kHz. The FFT block size used was 8192 and the resolution frequency was 9.76 Hz. Approximately 10–12 s of data were analyzed.

The normal force coefficient spectra show that the pressure field contains energy over a moderately wide frequency range. A peak in the power spectral density can be detected for all the three angles of attack investigated. The center frequency changes slightly with angle of attack. The reduced frequency decreases with α from 0.49 at α = 25 deg to 0.45 at α = 35 deg.

Investigation of the pressures in the vortical flowfield[3] behind the vertical fin carried out using a pitot-pressure rake also shows the pressure power spectral density curves to have similar shapes as those for the buffet loads. Experiments[2] carried out with the tail section removed give similar power

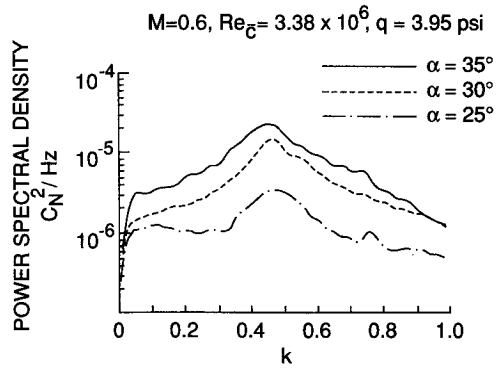

Fig. 13 Power spectral density of buffet load.

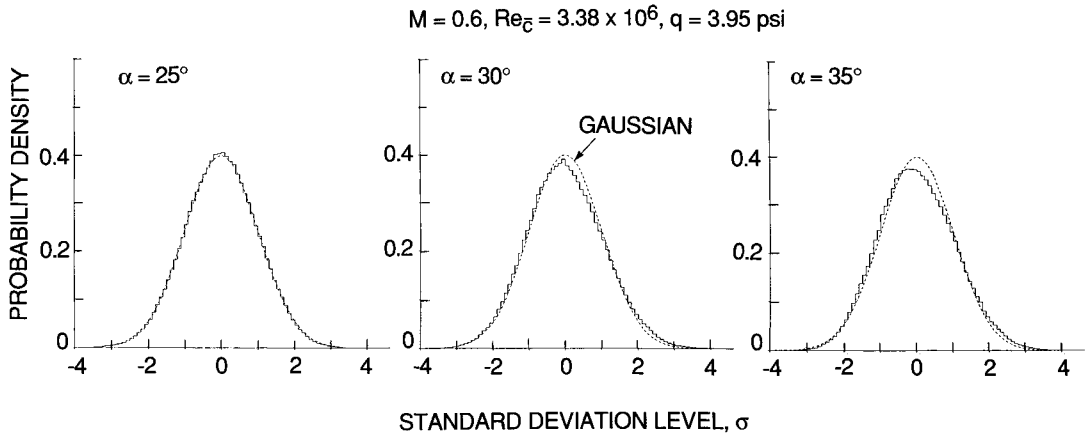

Fig. 14 Probability density of buffet load.

spectral density curves and the same values of center frequency. The peak in the buffet load spectra is a property of the flowfield. It is not due to structural effects related to flow interactions with the vertical fin. The observed center frequency is probably associated with some characteristic frequency present in the flowfield generated as a result of the LEX vortex bursting. Up to the present time, there is no experimental evidence that a discrete frequency can be produced nor is there a theory of the mechanism whereby such a frequency can be generated. Further investigation of the vortex burst phenomenon is required to explain this important observation. For a flexible aircraft, the presence of a peak in the load power spectra which varies with frequency, dynamic pressure, and angle of attack[6,13] can result in large structural response. This occurs when the peak frequency in the buffet loads and one of the fin natural frequency approximately coincide with each other. However, the dynamic response can be minimized by choosing the structural properties so that tuning of the peak in the buffet load spectra with any one of the natural frequencies of the vertical fin is avoided.

Another useful statistical property of the buffet loads for structural analysis is the probability density distribution. Figure 14 shows that the Gaussian distribution is a good representation of the normal force probability density function at $\alpha = 25, 30$, and 35 deg. The deviation from a Gaussian process increases slightly with increasing angle of attack. Analysis of the pressure transducer signals on the fin surfaces show that the probability density functions are also approximately Gaussian at most of the transducer positions. At $\alpha = 25$ deg, there are a number of transducers located below the 50% span line on both surfaces that show a slightly larger probability density at the zero standard deviation level. At $\alpha = 30$ deg, some of the transducers located about midspan on the inboard fin surface show a small shift of the maximum peak to either side of the Gaussian distribution curve. The magnitude of this shift increases at $\alpha = 35$ deg.

Reference 3 reported that from the pitot-pressure rake measurements, most of the pressure transducer signals in the flowfield behind the vertical fin have probability densities that are approximately Gaussian. There are only a few positions near the aircraft surface where a Gaussian approximation is not accurate. The present results and those given in Ref. 3 suggest that the pressures in the vortical flowfield around the vertical fin and those on the fin surfaces have similar statistical properties. This is a useful finding since it may be possible to use measurements of the properties of the flowfield to predict the pressures on the fin. This will result in eliminating the cost of installation of instruments on the fin. Some investigation in the correlation of the pressure fluctuations in the vortical flowfield with the fin unsteady pressures is in progress.

IV. Conclusions

Time-averaged and rms pressures on the vertical fin surfaces of a rigid 6% scale model of the F/A-18 due to buffet were investigated at $M = 0.6$ and $\alpha = 25$, 30, and 35 deg. The time-averaged pressure distributions at $\alpha = 30$ and 35 deg are quite similar on the inboard surface. On the outboard surface, the pressures at $\alpha = 25$ deg are larger than those at $\alpha = 30$ and 35 deg. The rms values of the unsteady pressure fluctuations increase with increasing α on both surfaces of the fin. Space-time broadband correlation of the pressure field shows that the convection pattern is very different on the fin surfaces. At $\alpha = 30$ deg, the eddy scale on the inboard surface is found to be larger than that on the outboard surface. Spectral analyses of the vertical fin buffet loads show a broad peak at a value of reduced frequency which varies with angle of attack. The value decreases from 0.49 at $\alpha = 25$ deg to 0.45 at $\alpha = 35$ deg. The probability density function of the buffet load shows that it has practically a Gaussian distribution at $\alpha = 25$ deg and there is a small deviation from the Gaussian profile when the angle of attack is increased.

Acknowledgments

The wind-tunnel program was funded in part by the Department of National Defense. The authors are indebted to the Institute for Aerospace Research for support in the high-angle-of-attack research project.

References

[1]Lee, B. H. K., Brown, D., Zgela, M., and Poirel, D., "Wind Tunnel Investigation and Flight Tests of Tail Buffet on the CF-18 Aircraft," Aircraft Dynamic Loads Due to Flow Separation, Paper 1, AGARD-CP-483, Sorrento, Italy, April, 1990.

[2]Lee, B. H. K., and Brown, D., "Wind Tunnel Studies of F/A-18 Tail Buffet," *Journal of Aircraft*, Vol. 29, No. 1, 1992, pp. 146–152.

[3]Lee, B. H. K., Brown, D., Tang, F. C., and Plosenski, M., "Flowfield in the Vicinity of the F/A-18 Vertical Fin at High-Angle-of-Attack," *Journal of Aircraft*, Vol. 30, No. 1, 1993, pp. 69–74.

[4]Lee, B. H. K., and Dunlavy, S., "Statistical Prediction of Maximum Buffet Loads on the F/A-18 Vertical Fin," *Journal of Aircraft*, Vol. 29, No. 4, 1992, pp. 734–736.

[5]Erickson, G. E., Hall, R. M., Banks, D. W., Del Frate, J. H., Schreiner, J. A., Hanley, R. J., and Pulley, C. T., "Experimental Investigation of the F/A-18 Vortex Flows at Subsonic Through Transonic Speeds, Invited Paper," AIAA 7th Applied Aerodynamics Conf., AIAA Paper 89-2222, Seattle, WA, July–Aug. 1989.

[6]Ferman, M. A., Patel, S. R., Zimmerman, N. H., and Gerstenkorn, G., "A Unified Approach to Buffet Response of Fighter Aircraft Empennage," *Aircraft Dynamic Loads Due to Flow Separation*, Paper 2, AGARD-CP-483, Sorrento, Italy, April, 1990.

[7]Lee, B. H. K., "A Method for Predicting Wing Response to Buffet Loads," *Journal of Aircraft*, Vol. 21, No. 1, 1984, pp. 85–87.

[8]Lee, B. H. K., and Tang, F. C., "Buffet Load Measurements on an F/A-18 Vertical Fin at High-Angle-of-Attack," AIAA Dynamics Specialists Conf., AIAA Paper 92-2127, Dallas, TX, April 16–17, 1992.

[9]Fisher, D. F., Del Frate, J. H., and Zuniga, F. A., "Summary of In-Flight Flow Visualization Obtained from the NASA High Alpha Research Vehicle," NASA TM-101734, Jan. 1991.

[10]Rabiner, L. R., Schafer, R. W., and Dlugos, D., "Chapter 2.1, Periodgram Method for Power Spectrum Estimation," "Chapter 2.3, A Coherence and Cross Spectral Estimation Program," *Programs for Digital Signal Processing*, edited by The Digital Signal Processing Committee, IEEE Acoustics, Speech and Signal Processing Society, IEEE Press, New York, 1979.

[11]Meyn, L. A., Lanser, W. R., and James, K. D., "Full-Scale High Angle-of-Attack Tests of an F/A-18," AIAA 10th Applied Aerodynamics Conf., AIAA Paper 92-2676, Palo Alto, CA, June 22–24, 1992.

[12]Lee, B. H. K., and Tang, F. C., "Unsteady Pressure and Load Measurements on an F/A-18 Vertical Fin at High-Angle-of-Attack," AIAA 10th Applied Aerodynamics Conf., AIAA Paper 92-2675, Palo Alto, CA, June 22–24, 1992.

[13]Martin, C. A., and Thompson, D. H., "Scale Model Experiments of Fin Buffet Due to Vortex Bursting on F/A-18," *Manoeuvring Aerodynamics*, AGARD-CP-497, Toulouse, France, May 1–2, 1991.